Reversible Osmium(VI) Nitrido to Osmium(II) Ammine Interconversion in Complexes Containing Polypyrazolyl Ligands†

El-Sayed El-Samanody,‡ Konstantinos D. Demadis,§ Thomas J. Meyer,*,|| and Peter S. White⊥

Department of Chemistry, Venable and Kenan Laboratories, CB 3290, University of North Carolina at Chapel Hill, Chapel Hill, North Carolina 27599-3290, and Los Alamos National Laboratory, P.O. Box 1663, MS A127, Los Alamos, New Mexico 87545

Received July 11, 2000

This paper describes the $4e^-/3H^+$ interconversion between NH_3 and N^{3-}, which is reversible in the coordination spheres of Os complexes containing either tpm (tpm = tris(1-pyrazolyl)methane) or Tp (Tp = hydrotris(1-pyrazolyl)-borate anion) ligands. Electrochemical or chemical reduction of the nitrido complexes $[Os^{VI}(tpm)(Cl)_2(N)]^+$ (**1**) and $Os^{VI}(Tp)(Cl)_2(N)$ (**2**) in acidic aqueous solution gives the corresponding Os^{II}−ammine complexes, which, after air oxidation and workup, are isolated and structurally characterized as $[Os^{III}(tpm)(Cl)_2(NH_3)](PF_6)$ (**3**) and $Os^{III}(Tp)(Cl)_2(NH_3)$ (**4**). The Os^{III}−ammine complexes are reoxidized electrochemically to the nitrido complexes by stepwise mechanisms involving the loss of both electrons and protons and sequential Os(III→IV) and Os(IV→VI) oxidations.

Introduction

The interconversion of bound nitrogen from nitrosyl/nitrite to NH_3 has been studied in polypyridyl complexes of Ru and Os such as $[M^{II}(tpy)(bpy)(NO)]^{3+}$ (tpy = 2,2′:6′,2″-terpyridine; bpy = 2,2′-bipyridine; M = Ru or Os).[1] In aqueous solution, reversible interconversion between Os^{III}−ammine and Os^{VI}−nitrido complexes has been observed.[2a,3]

$$[Os^{III}(tpy)(Cl)_2(NH_3)]^+ \underset{+3e^-,\,3H^+}{\overset{-3e^-,\,3H^+}{\rightleftharpoons}} [Os^{VI}(tpy)(Cl)_2(N)]^+ \quad (1)$$

At pH 9, competitive oxidation of *cis*-$[Os^{II}(bpy)_2(Cl)(NH_3)]^+$ gives a μ-N_2 and nitrosyl products[3]

$$2cis\text{-}[Os^{II}(bpy)_2(Cl)(NH_3)]^+ \xrightarrow{-6e^-,\,-6H^+} cis,cis\text{-}[(bpy)_2(Cl)Os^{II}(N_2)Os^{II}(Cl)(bpy)_2]^{2+} \quad (2)$$

$$cis\text{-}[Os^{II}(bpy)_2(Cl)(NH_3)]^+ \xrightarrow[+H_2O]{-6e^-,\,-5H^+} cis\text{-}[Os^{II}(bpy)_2(Cl)(NO)]^{2+} \quad (3)$$

Buhr and Taube found a related reactivity in a series of Os−ammine complexes.[4]

These reactions appear to proceed through deprotonated Os^{IV} intermediates, which undergo further oxidation, proton loss, and hydration to give nitrosyls. Although stable, deprotonated Os^{IV} intermediates have not been isolated. They can be trapped in the oxidation of $[Os^{III}(tpy)(bpy)(NH_3)]^{3+}$ by secondary amines to give Os(IV)−hydrazido products, $[Os^{IV}(tpy)(bpy)(NNR_2)]^{2+}$.[5]

In more electron-rich coordination environments, Os^{VI}−nitrido complexes are accessible by ligand substitution in $[Os^{VI}(N)(Cl)_4]^-$ (eq 4).[6]

$$[N(Bu)_4][Os^{VI}(N)(Cl)_4] + L_3 \rightarrow [Os^{VI}(L_3)(Cl)_2(N)]Cl + [N(Bu)_4]Cl \quad (4)$$

L_3 = neutral tridentate ligand

The nitrido complex $[Os^{VI}(tpm)(Cl)_2(N)]^+$ (tpm = tris(1-pyrazolyl)methane) has an extensive reactivity with N_3^- to give $Os^{II}(tpm)(Cl)_2(N_2)$,[7] with CS_2 in the presence of N_3^- to give $[Os^{II}(tpm)(Cl)_2(NS)]^+$,[7,8] toward one-electron reduction followed by N···N coupling to give $(tpm)(Cl)_2Os^{II}(N_2)Os^{II}(Cl)_2(tpm)$,[9]

† This paper is dedicated to Professor Dimitri Coucouvanis on the occasion of his 60th birthday.

* Corresponding author e-mail: tjmeyer@lanl.gov.

‡ On leave from the Department of Chemistry, Menoufia University, Shebin El-Kom, Egypt.

§ Present address: Specialty Division Research, Nalco Chemical Company, a Suez Lyonnaise Des Eaux Company, One Nalco Center, Naperville, IL 60563-1198. E-mail: nitrido@onebox.com.

|| Los Alamos National Laboatory.

⊥ University of North Carolina at Chapel Hill, UNC-Chemistry departmental crystallographer.

(1) (a) Murphy, W. R., Jr.; Takeuchi, K. J.; Meyer, T. J. *J. Am. Chem. Soc.* **1982**, *104*, 517. (b) Pipes, D. W.; Meyer, T. J. *Inorg. Chem.* **1984**, *23*, 2466. (c) Ooyama, D.; Nagao, H.; Ito, K.; Nagao, N.; Howell, F. S.; Mukaida, M. *Bull. Chem. Soc. Jpn.* **1997**, *70*, 2141.

(2) Pipes, D. W.; Bakir, M.; Vitols, S. E.; Hodgson, D. J.; Meyer, T. J. *J. Am. Chem. Soc.* **1990**, *112*, 5507.

(3) (a) Coia, G. M.; Demadis, K. D.; Meyer, T. T. *Inorg. Chem.* **2000**, *39*, 2212. (b) Coia, G. M. Ph.D. Dissertation, The University of North Carolina, Chapel Hill, 1996.

(4) Buhr, J. D.; Winkler, J. R.; Taube, H. *Inorg. Chem.* **1980**, *19*, 2416.

(5) (a) Coia, G. M.; White, P. S.; Meyer, T. J.; Wink, D. A.; Keefer, L. K.; Davis, W. M. *J. Am. Chem. Soc.* **1994**, *116*, 3649. (b) Coia, G. M.; Wink, D. A.; Devenney, M.; White, P. S.; Meyer, T. J. *Inorg. Chem.* **1997**, *36*, 2341.

(6) (a) Ware, D. C.; Taube, H. *Inorg. Chem.* **1991**, *30*, 4598. (b) Griffith, W. P.; Pawson, D. *J. Chem. Soc., Dalton Trans.* **1975**, 416. (c) Wright, H. J.; Griffith, W. P. *Transition Met. Chem.* **1982**, *7*, 53. (d) Sen, D.; Ta, N. C. *Indian J. Chem.* **1978**, *16A*, 859. (e) Newton, C.; Edwards, K. D.; Ziller, J. W.; Doherty, N. M. *Inorg. Chem.* **1999**, *38*, 4032. (f) Griffith, W. P. *Coord. Chem. Rev.* **1972**, *8*, 369.

(7) Demadis K. D.; El-Samanody, E.-S.; Meyer, T. J.; White, P. S. *Inorg. Chem.* **1998**, *37*, 838.

(8) El-Samanody, E.-S.; Demadis, K. D.; Gallagher, L. A.; Meyer, T. J.; White, P. S. *Inorg. Chem.* **1998**, *38*, 3329.

(9) Demadis, K. D.; El-Samanody, E.-S.; Coia, G. M.; Meyer, T. J. *J. Am. Chem. Soc.* **1999**. *121*, 535.

10.1021/ic000764f CCC: $20.00
Published on Web 06/14/2001

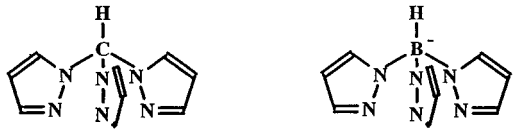

tpm **Tp**

Figure 1. Ligand structures, tpm = tris(1-pyrazolyl) methane; Tp^- = hydridotris(1-pyrazolyl)borate anion.

Scheme 1

$[Os^{VI}(tpm)(Cl)_2(N)](PF_6)$	**(1a)**
$[Os^{VI}(tpm)(Cl)_2(N)](BF_4)$	**(1b)**
$[Os^{VI}(tpm)(Cl)_2(^{15}N)](PF_6)$	**(1*a)**
$Os^{VI}(Tp)(Cl)_2(N)$	**(2)**
$Os^{VI}(Tp)(Cl)_2(^{15}N)$	**(2*)**
$[Os^{III}(tpm)(Cl)_2(NH_3)](PF_6)$	**(3)**
$Os^{III}(Tp)(Cl)_2(NH_3)$	**(4)**

with secondary amines to give $[Os^{V}(tpm)(Cl)_2(NNR_2)]^+$,[10] and with PPh_3 to give $[Os^{IV}(tpm)(Cl)_2(NPPh_3)]^+$.[11]

In this paper, we report an extension of earlier work on reversible Os^{VI}−nitrido to Os^{II}−ammine interconversion, in this case to $[Os^{VI}(tpm)(Cl)_2(N)]^+$ and $Os^{VI}(Tp)(Cl)_2(N)$ (Tp = hydridotris(1-pyrazolyl)borate anion). This work provides additional insight into how these reactions occur. Structures of the tpm and Tp ligands are shown in Figure 1.

Experimental Section

The compounds and salts that appear in this study are shown in Scheme 1. Abbreviations used in the text include tpm = tris(1-pyrazolyl)methane, TBAH = tetrabutylammonium hexafluorophosphate, Tp^- = hydridotris(1-pyrazolyl)borate anion, tpy = 2,2′:6′,2″-terpyridine, and bpy = 2,2′-biprydine.

Materials. Osmium tetraoxide (>99%) and potassium hydridotris-(1-pyrazolyl)borate were obtained from Alfa-AESAR, and $^{15}NH_4Cl$ (>99%) was from Aldrich. All other chemicals were of reagent grade and used without further purification.

Measurements. Electronic absorption spectra were acquired by using a Hewlett-Packard model 8452A diode array spectrophotometer. FT-IR spectra were recorded on a Mattson Galaxy series 5000 instrument at 4 cm^{-1} resolution. Proton NMR spectra were recorded on a Bruker AC200 (200 MHz) spectrometer. Elemental analyses were performed by Oneida Research Services, Inc. (Whitesboro, NY). Electrochemical measurements were conducted by using a PAR model 273 potentiostat. For aqueous voltammetry, a 3.0 mm diameter glassy carbon disk working electrode (Bioanalytical Systems, West Lafayette, IN) and a saturated sodium chloride calomel reference electrode (SSCE) were used. For nonaqueous measurements, the working electrode was a 1.0 mm platinum disk, and the reference was a silver wire immersed in a CH_3CN solution that was 0.01 M in $AgNO_3$ and 0.1 M in TBAH. In all cases, the auxiliary electrode was a coil of platinum wire. Three-compartment cells were used with sintered glass disks separating the compartments containing reference, working, and auxiliary electrodes. The solution of the working compartment was deoxygenated with a stream of nitrogen. Buffers for aqueous voltammetry were prepared by neutralizing solutions of reagent A (listed below) with solid or concentrated reagent B until the desired pH was reached. For pH 9.2−10.80, A = 0.025 M $Na_2B_4O_7\cdot10H_2O$ and B = 0.1 M NaOH; for pH 8.0−9.1, A = 0.025 M $Na_2B_4O_7\cdot10H_2O$ and B = 0.1 M HCl; for pH 5.8−8.0, A = 0.025 M NaH_2PO_4 and B = 0.1 M NaOH; for pH 2.2−4.0, A = 0.1 M potassium hydrogen phthalate and B = 0.1 M HCl. Solutions of pH <1 were prepared by diluting concentrated H_2SO_4.

Synthesis and Characterization. The following salts and compounds were prepared by literature procedures: $K[OsO_3N]$,[12] $K[OsO_3{}^{15}N]$,[12] $[N(Bu)_4][Os(N)(Cl)_4]$,[13] $[N(Bu)_4][Os(^{15}N)(Cl)_4]$,[13] $Os^{VI}(Tp)(Cl)_2(N)$,[14] and tpm.[15]

$[Os^{VI}(tpm)(Cl)_2(N)](PF_6)$ (1a). A quantity of $[N(Bu)_4][Os(N)(Cl)_4]$ (1.00 g, 1.69 mmol) and tpm (0.40 g, 1.86 mmol) were mixed together in CH_3OH (50 mL). The reaction mixture was stirred overnight, during which time the color turned to pink-orange. NH_4PF_6 (1.00 g) was added as a solid to the reaction mixture. An orange solid precipitated and was filtered off, washed with EtOH, recrystallized from CH_3CN/Et_2O, and finally air-dried. Yield: 0.75 g (70%). Anal. Calcd for $C_{10}H_{10}Cl_2N_7OsPF_6$ (mol wt 634.96): C, 18.90; H, 1.59; N, 15.44. Found: C, 19.29; H, 1.73; N, 15.61. UV−Vis (CH_3CN) λ_{max}, nm (ϵ, M^{-1} cm^{-1}): 446 (200), 270 (14 500), 250 (14 500), 212 (16 300). IR (cm^{-1}, KBr disks): ν(Os≡N) 1074; ν(tpm) 1515, 1446, 1409, 1285; ν(P−F) 835. ^1H NMR (200 MHz, CD_3CN, δ): 6.33 (t, 1H), 6.88 (t, 2H), 7.59 (d, 1H), 8.14 (d, 1H), 8.54 (d, 2H), 8.65 (d, 2H), 9.17 (s, 1H).

$[Os^{VI}(tpm)(Cl)_2(^{15}N)](PF_6)$ (1*a). This salt was prepared the same as for **1a** except that $[N(Bu)_4][Os(^{15}N)(Cl)_4]$ was used as the starting material. IR (cm^{-1}, KBr disks): ν(Os≡^{15}N) 1053 (vs).

$[Os^{VI}(tpm)(Cl)_2(N)](BF_4)$ (1b). The BF_4^- salt was prepared the same as for **1a** except that $NaBF_4$ was added to the reaction mixture rather than PF_6^-. Yield: 0.50 g (51%). Anal. Calcd for $C_{10}H_{10}Cl_2N_7OsBF_4$ (mol wt 577.0): C, 20.80; H, 1.75; N, 16.99. Found: C, 21.46; H, 1.55; N, 16.82.

$[Os^{III}(tpm)(Cl)_2(NH_3)](PF_6)$ (3). A quantity of **1a** (260 mg, 0.4 mmol) was suspended in 50 mL of 3 M HCl. Several pieces of amalgamated zinc were added, and the mixture was stirred vigorously in a stoppered flask. The suspension became pale yellow, and a yellow precipitate formed. After 30 min, the zinc was removed. The reaction mixture was further stirred for 1 h, and the yellow precipitate redissolved to form a clear yellow solution. Solid NH_4PF_6 (5.0 g) was added, and the mixture was chilled to 0 °C and stirred for 1 h. The tan product was collected by filtration, recrystallized from CH_3CN/Et_2O, and dried. Yield: 96 mg (36%). Anal. Calcd for $C_{10}H_{13}Cl_2N_7OsPF_6$ (mol wt 637.98): C, 18.81; H, 2.05; N, 15.36. Found: C, 18.57; H, 1.83; N, 14.91. UV−Vis (CH_3CN) λ_{max}, nm (ϵ, M^{-1} cm^{-1}): 320 (6600), 290 (9050), 204 (12 560). IR (cm^{-1}, KBr disks): ν(N−H) 3338, 3256; ν(tpm) 1512, 1445, 1409, 1279; ν(P−F) 850.

$Os^{III}(Tp)(Cl)_2(NH_3)$ (4). A quantity of **2** (150 mg, 0.30 mmol) was dissolved in 20 mL of CH_3OH, and 3 equiv of $SnCl_2\cdot2H_2O$ (207 mg, 0.92 mmol) was added as a solid followed by 7 drops of concentrated HCl. The resulting reaction mixture was stirred for 3 h, and the color turned from red to yellow. The volume was reduced to 2 mL by rotary evaporation, and the orange precipitate was filtered off, washed with 1 mL of CH_3OH and 20 mL of Et_2O, and air-dried. Yield: 86 mg (57%). Anal. Calcd for $C_9H_{13}Cl_2N_7OsB$ (mol wt 492.0): C, 21.95; H, 2.66; N, 19.92. Found: C, 21.26; H, 2.56; N, 19.62. UV−Vis (CH_3CN) λ_{max}, nm (ϵ, M^{-1} cm^{-1}): 318 (5000), 278 (9000), 248 (7200), 202 (11 350). IR (cm^{-1}, KBr disks): ν(N−H) 3289, 3220, 3156; ν(B−H) 2486; ν(Tp) 1620, 1498, 1405, 1310, 1209.

X-ray Structural Determinations. Data Collection, Solution, and Refinement of the Structures. Single crystals of **1b**, the BF_4^- salt of **1**, were obtained by slow diffusion of Et_2O into a CH_3CN solution of the salt. Single crystals of **3** as PF_6^- salt **3** were obtained by slow precipitation of the compound from a concentrated aqueous solution containing $NaPF_6$. Single crystals of **4** were obtained by slow diffusion of Et_2O into a DMF solution of the compound. Crystal data, intensity

(10) (a) Huynh, M. H. V.; El-Samanody, E.-S.; Demadis, K. D.; Meyer, T. J.; White, P. S. *J. Am. Chem. Soc.* **1999**, *121*, 1403. (b) Huynh, M. H. V.; El-Samanody, E.-S.; Demadis, K. D.; White, P. S.; Meyer, T. J. *Inorg. Chem.* **2000**, *122*, 3075.

(11) El-Samanody, E.-S.; Huynh, M. H. V.; Demadis, K. D.; Meyer, T. J.; White, P. S. Manuscript in preparation.

(12) Clifford, A. F.; Kobayashi, C. S. *Inorg. Synth.* **1960**, *6*, 204.

(13) Cowman, C. D.; Trogler, w. C.; Mann, K. R.; Gray, H. B. *Inorg. Chem.* **1976**, *15*, 1749.

(14) Byers, P. K.; Canty, A. J.; Honeyman, R. T. *J. Organomet. Chem.* **1990**, *385*, 421.

(15) (a) Crevier, T. J.; Mayer, J. M. *J. Am. Chem. Soc.* **1998**, *120*, 5595. (b) Crevier, T. J.; Lovell, S.; Mayer, J. M.; Rheingold, A. L.; Guzei, I. A. *J. Am. Chem. Soc.* **1998**, *120*, 6607.

Table 1. Summary of Crystal Data, Intensity Collection, and Structure Refinements Parameters for **1b**, **3**, and **4**

compound	**1b**	**3**	**4**
formula	$OsCl_2C_{10}H_{10}BF_4N_7$	$OsCl_2C_{10}H_{13}PF_6N_7.0.5H_2O$	$OsCl_2C_9H_{13}BN_7.0.5DMF$
mol wt	609.32	646.33	525.65
a (Å)	21.654(5)	15.1206(8)	22.9011(13)
b (Å)	8.658(3)	19.6587(11)	10.1306(6)
c (Å)	18.638(8)	12.4379(9)90	15.0047(8)
γ (deg)	90	90	90
β (deg)	101.41(5)	90	108.343(1)
γ (deg)	90	90	90
V (Å^3)	3425(2)	3697.2(4)	3304.2(3)
Z	8	8	8
cryst color and habit	red needles	yellow plates	yellow blocks
cryst syst	monoclinic	orthorombic	monoclinic
space group	*C2/c*	*Ccmm*	*C2/c*
cryst size (mm)	0.25 × 0.30 × 0.30	0.35 × 0.25 × 0.25	0.25 × 0.25 × 0.10
d_{calcd} (g/cm^3)	2.363	2.322	2.113
diffractometer	Rigaku	Siemens CCD Smart	Siemens CCD Smart
radiation	Mo Kα (λ = 0.71073 Å)	Mo Kα (λ = 0.71073 Å)	Mo Kα (λ = 0.71073 Å
collection *T* (°C)	−100	−180	−100
abs coeff μ, cm^{-1}	8.43	7.34	8.05
F(000)	2269.38	2446.03	1996.19
$2\theta_{max}$ (deg)	50.0	50.5	60.0
total reflns	3463	16993	12530
unique reflns	2903	1771	4715
refined reflns	2017	1722	3876
merging *R* value	0.040	0.021	0.021
no. of params	227	162	215
R (%)[a]	6.0	2.6	3.0
Rw (%)[b]	7.0	2.6	3.1
GOF[c]	2.04	6.11	2.29
deepest hole (e/Å^3)	−4.490	−0.900	−1.940
highest peak (e/Å^3)	3.390	1.610	1.620

[a] $R = \sum(|F_o - F_c|)/\sum|F_o|$. [b] $Rw = [\sum(w|F_o - F_c|)^2/\sum w(F_o)^2]^{1/2}$. [c] $GOF = [\sum w(F_o - F_c)^2/(\text{no. of reflections} - \text{no. of parameters})]^{1/2}$.

collection information, and structure refinement parameters for the structures are provided in Table 1. The structures were solved by direct methods. The remaining non-hydrogen atoms were located in subsequent difference Fourier maps. Empirical absorption corrections were applied with SADABS. The ORTEP plotting program was used to computer generate the structures shown in Figures 2−4.[16] Hydrogen atoms were included in calculated positions with thermal parameters derived from the atom to which they were bonded. All computations were performed by using the NRCVAX suite of programs.[17] Atomic scattering factors were taken from a standard source[18] and corrected for anomalous dispersion.

A chloride ligand and the nitrido ligands in the crystal of **1b** exhibit random disorder. Cl/N(2) and Cl/N(3) represent sites occupied randomly by Cl and N. Attempts to distinguish the individual Cl and N positions were unsuccessful. The structure of **3** contains one-half molecule of H_2O, which is hydrogen bonded to the ammine N. The PF_6^- counterion was disordered, but this disorder was modeled successfully. The structure of **4** contains a molecule of DMF disordered about a 2-fold axis. This corresponds to 0.5 DMF per molecule.

The final positional parameters along with their standard deviations as estimates from the inverse matrix, tables of hydrogen atom parameters, anisotropic thermal parameters, and observed/calculated structure amplitudes for **1b**, **3**, and **4** are available as Supporting Information. Selected bond lengths (Å) and angles (deg) for **1b**, **3**, and **4** are given in Table 2.

Results

Synthesis. The reaction between $[N(Bu)_4](Os(N)(Cl)_4]$ and the facial tridentate ligand tpm in CH_3OH occurs with Cl^- displacement to give $[Os^{VI}(tpm)(Cl)_2(N)](Cl)$, as in eq 5.

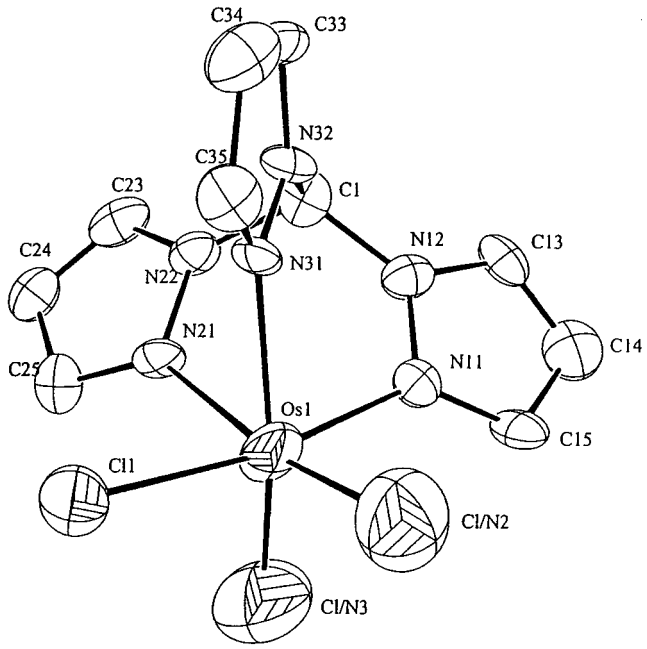

Figure 2. ORTEP diagram of the cation (40% probability ellipsoids) $[Os^{VI}(tpm)(Cl)_2(N)]^+$ in **1b**.

Addition of either NH_4PF_6 or $NaBF_4$ in excess caused precipitation of the orange salts, **1a** or **1b**, in 70−75% yield.

$$[N(Bu)_4](Os^{VI}(N)(Cl)_4] + tpm \xrightarrow{CH_3OH} [Os^{VI}(tpm)(Cl)_2(N)]Cl + [N(Bu)_4]Cl \quad (5)$$

The Os^{III}−ammine salts, **3** and **4**, were prepared by chemical reduction of the corresponding Os^{VI}−nitrido complexes **1a** and

(16) Johnson, C. K. *ORTEP*: *A Fortran Thermal Ellipsoid Plot Program*; Technical Report ORNL-5138; Oak Ridge National Laboratory: Oak Ridge, TN, 1976.
(17) Gabe, E. J.; Le Page, Y.; Charland, J.-P.; Lee, F. L.; White, P. S. *J. Appl. Crystallogr*. **1989**, *22*, 384.
(18) *International Tables for X-ray Crystallography*; Kynoch Press: Birmigham, U.K., 1974; Vol. IV.

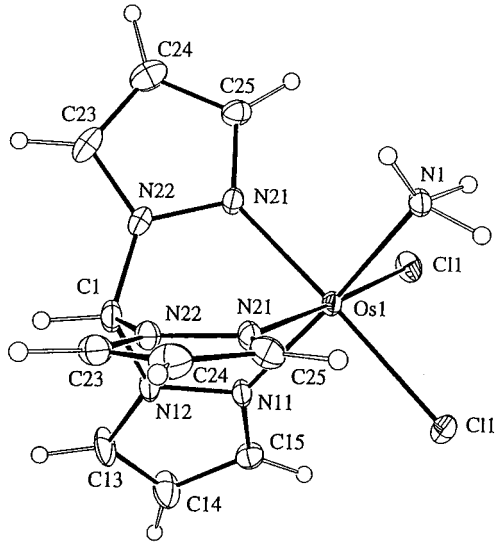

Figure 3. ORTEP diagram (40% probability ellipsoids) of the cation $[Os^{III}(tpm)(Cl)_2(NH_3)]^+$ in **3**.

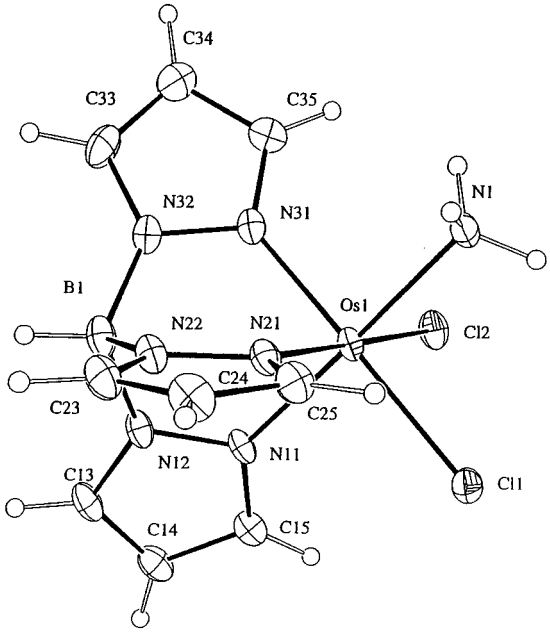

Figure 4. ORTEP diagram (40% probability ellipsoids) of **4**.

2. For the reduction of **1a**, amalgamated Zn in acidic aqueous solution was used as the reductant to give $Os^{II}(tpm)(Cl)_2(NH_3)$, which is air oxidized during workup to give the cation of **3** (eq 6). Addition of excess NH_4PF_6 caused precipitation of the PF_6^- salt.

$$[Os^{VI}(tpm)(Cl)_2(N)]^+ \xrightarrow[O_2]{Zn(Hg),\ H^+} [Os^{III}(tmp)(Cl)_2(NH_3)]^+ \quad (6)$$

2 was reduced by $SnCl_2 \cdot 2H_2O$ in acidic CH_3OH solution to give **4** (eq 7). Both reactant and product are nonelectrolytes and are sparingly soluble in CH_3OH. **4** was conveniently separated from Sn^{IV} by filtration. The solubility of **4** in polar organic solvents allowed its purification by recrystallization from CH_3CN/Et_2O mixtures.

$$Os^{VI}(Tp)(Cl)_2(N) \xrightarrow[MeOH,\ O_2]{SnCl_2,\ H^+} Os^{III}(Tp)(Cl)_2(NH_3) \quad (7)$$

Table 2. Selected Bond Distances (Å) and Angles (deg) for **1b** (Labeling Scheme as in Figure 2), **3** (Figure 3), and **4** (Figure 4)

$[Os^{III}(tpm)(Cl)_2(N)]^+$ (**1b**)

Bond Lengths (Å)

Os(1)−Cl(1)	2.399(4)	Os(1)−N(11)	2.122(11)
Os(1)−Cl/N(2)	2.151(7)	Os(1)−N(21)	2.229(11)
Os(1)−Cl/N(3)	1.887(10)	Os(1)−N(31)	2.172(12)

Bond Angles (°)

Cl(1)−Os(1)−Cl/N(2)	94.8(2)	Cl/N(2)−Os(1)−N(31)	93.1(4)
Cl(1)−Os(1)−Cl/N(3)	93.2(3)	Cl/N(3)−Os(1)−N(11)	94.6(4)
Cl(1)−Os(1)−N(11)	169.9(3)	Cl/N(3)−Os(1)−N(21)	92.3(4)
Cl(1)−Os(1)−N(21)	87.1(3)	Cl/N(3)−Os(1)−N(31)	168.8(4)
Cl(1)−Os(1)−N(31)	86.2(3)	N(11)−Os(1)−N(21)	86.2(4)
Cl/N(2)−Os(1)−Cl/N(3)	98.1(3)	N(11)−Os(1)−N(31)	84.9(4)
Cl/N(2)−Os(1)−N(11)	90.4(4)	N(21)−Os(1)−N(31)	76.5(4)
Cl/N(2)−Os(1)−N(21)	169.3(4)		

$[Os^{III}(tpm)(Cl)_2(NH_3)]^+$ (**3**)

Bond Lengths (Å)

Os(1)−Cl(1)	2.3458(10)	Os(1)−N(11)	2.056(5)
Os(1)−Cl(1)a	2.3458(10)	Os(1)−N(21)	2.065(3)
Os(1)−N(1)	2.101(5)	Os(1)−N(21)a	2.065(3)

Bond Angles (°)

Cl(1)−Os(1)−Cl(1)[a]	91.32(4)	Cl(1)a-Os(1)−N(21)[a]	91.46(10)
Cl(1)−Os(1)−N(1)	89.34(9)	N(1)−Os(1)−N(11)	174.97(18)
Cl(1)−Os(1)−N(11)	94.17(10)	N(1)−Os(1)−N(21)	90.76(13)
Cl(1)−Os(1)−N(21)	91.46(10)	N(1)−Os(1)−N(21)[a]	90.76(13)
Cl(1)−Os(1)−N(21)a	177.21(10)	N(11)−Os(1)−N(21)	85.55(13)
Cl(1)a-Os(1)−N(1)	89.34(9)	N(11)−Os(1)−N(21)[a]	85.55(13)
Cl(1)a-Os(1)−N(11)	94.17(10)	N(21)−Os(1)−N(21)[a]	85.75(13)
Cl(1)a-Os(1)−N(21)	177.21(10)		

$Os^{III}(Tp)(Cl)_2(NH_3)$ (**4**)

Bond Lengths (Å)

Os(1)−Cl(1)	2.371(1)	Os(1)−N(11)	2.065(3)
Os(1)−Cl(2)	2.382(1)	Os(1)−N(21)	2.050(4)
Os(1)−N(1)	2.133(3)	Os(1)−N(31)	2.054(4)

Bond Angles (°)

Cl(1)−Os(1)−Cl(2)	91.86(4)	Cl(2)−Os(1)−N(21)	178.48(10)
Cl(1)−Os(1)−N(1)	88.14(11)	Cl(2)−Os(1)−N(31)	91.37(11)
Cl(1)−Os(1)−N(11)	93.75(11)	N(1)−Os(1)−N(11)	178.05(13)
Cl(1)−Os(1)−N(21)	89.39(10)	N(1)−Os(1)−N(21)	94.00(14)
Cl(1)−Os(1)−N(31)	176.58(11)	N(1)−Os(1)−N(31)	90.91(14)
Cl(2)−Os(1)−N(1)	86.92(11)	N(11)−Os(1)−N(21)	85.54(14)
Cl(2)−Os(1)−N(11)	93.50(11)	N(11)−Os(1)−N(31)	87.17(15)

Similar methods have been used to reduce *cis*-$[Os^{VI}(tpy)(Cl)_2(N)]^+$ [3] and $Os^{VI}(py)_2(Cl)_3(N)$[6a] to give the corresponding Os^{III}−ammine complexes.

Molecular Structures. The crystal of **1b** contains discrete $[Os^{VI}(tpm)(Cl)_2(N)]^+$ cations (**1**) and BF_4^- anions. Because of disorder in the crystal between the nitrido N and a Cl ligand, it was not possible to obtain precise bond lengths, precluding a detailed description of the structure. However, the structure does reveal the ligand environment at the cation. The partial presence of nitrido N at Cl/N(3) causes the elongation in the Os−N(21) bond length of 2.229(11) Å, as compared to the other two Os−N(tpm) bonds because of the trans effect of the nitrido ligand.

The cation in **3** resides on a crystallographically imposed mirror plane including one pyrazole ring of tpm, Os, and the ammine N atom. The Os−N(NH_3) bond length is 2.101(5) Å, and the Os−N(tpm) bond lengths are 2.056(5) and 2.065(3) Å. The Os−Cl bond length of 2.3458(10) Å is comparable to Os−Cl in **4** (next paragraph). The H_2O molecule in the lattice acts as a bridge by forming hydrogen bonds between adjacent NH_3 ligands. The $O(H_2O)\cdots N(NH_3)$ contacts are 3.021(6) Å.

In the structure of **4**, the Os−N(Tp) bond lengths range from 2.050(4) to 2.065(3) Å. The Cl^- ligands are necessarily *cis* with

Os−Cl bond lengths of 2.3710(11) and 2.3824(13) Å, consistent with Os^{III}.[19] The Os−N(NH_3) bond length is 2.133(3) Å and is comparable to bond lengths in other M−NH_3 complexes.[20]

Spectroscopy. The ν(Os≡N) stretch commonly appears from 1000 to 1120 cm^{-1}.[6,21] In comparing the infrared spectra of **1a** and **1*a**, it is difficult to assign a band to the ν(Os≡N) mode because of the appearance of an intense ν(tpm) band at 1074 cm^{-1}. The only difference between ^{14}N and ^{15}N spectra is the appearance of a new band at 1053 cm^{-1} for the ^{15}N-labeled complex. For **2**,[14] $\nu(Os{\equiv}^{14}N)$ is observed at 1066 cm^{-1}, while for **2***, this band is replaced by a shoulder for $\nu(Os{\equiv}^{15}N)$ at 1033 cm^{-1}. For comparison, ν(Os≡N) has been reported at 1060 cm^{-1} in $Os^{VI}(py)_2(Cl)_3(N)$.[6a,c]

The IR spectra of Os^{III}−ammine complexes, **3** and **4**, reveal characteristic bands for coordinated NH_3.[22] For **3**, $\nu(NH_3)$ appears at 3338 and 3256 cm^{-1}. For **4**, $\nu(NH_3)$ appears at 3289, 3220, and 3156 cm^{-1}, and it is shifted to 2490 and 2321 cm^{-1} after partial H/D exchange. For comparison, $\nu(NH_3)$ has been reported at 3240 and 3160 cm^{-1} for $[Co(NH_3)_6]^{3+}$,[23] and $\nu(ND_3)$ has been reported at 2440 and 2300 cm^{-1} for $[Co(ND_3)_6]^{3+}$.[24] In the spectrum of **4**, ν(B−H) of the Tp ligand appears at 2486 cm^{-1}, and other Tp vibrations appear at 1620, 1498, 1405, 1310, and 1209 cm^{-1}.[13]

Ligand-based $\pi \rightarrow \pi^*$ bands appear in the UV−visible spectra of **1** and **2** measured in CH_3CN (data are summarized in Experimental Section). In addition, broad, weak bands appear in the visible region at 446 nm (ϵ = 200 M^{-1} cm^{-1}) for **1a** and at 452 nm (ϵ = 120 M^{-1} cm^{-1}) for **2**. Similar bands occur at 460 nm (ϵ = 280 M^{-1} cm^{-1}) and at 514 nm (ϵ = 120 M^{-1} cm^{-1}) for *cis*- and *trans*-$[Os^{VI}(tpy)(Cl)_2(N)]^+$, respectively, measured in CH_3CN.[25] In these d^2 Os^{VI} complexes, the electronic configuration is $d\pi_1^2 d\pi_2^0 d\pi_3^0$. If the *z*-axis is defined to lie along the Os−N bond, $d\pi_2$ and $d\pi_3$ are largely d_{xz} and d_{yz}. They have considerable Os−N antibonding character because of extensive mixing with the filled $2p_x$ and $2p_y$ orbitals of the nitrido ligand. Two interconfigurational $d\pi \rightarrow d\pi$ transitions are expected for this configuration, arising from the transitions $d\pi_1^2 d\pi_2^0 d\pi_3^0 \rightarrow d\pi_1^1 d\pi_2^1 d\pi_3^0$, $d\pi_1^1 d\pi_2^0 d\pi_3^1$. Although these transitions are normally parity forbidden, they gain intensity by spin−orbit coupling in the excited states.

In the ^1H NMR spectra of **1a** measured in CD_3CN, there is no evidence for paramagnetic broadening or shifts showing that these complexes are diamagnetic. The series of resonances that appear are characteristic of the coordinated tpm ligand.[26]

Electrochemistry in CH_3CN. In cyclic voltammograms of **1a** in 0.1 M TBAH/CH_3CN, an irreversible $Os^{VI/V}$ wave is observed at $E_{p,c} = -0.47$ V vs SSCE. In an oxidative scan following reduction past this wave, reversible waves appear at $E_{1/2} = +0.18$ and $+0.74$ V vs SSCE for the $Os^{III}-Os^{II}/Os^{II}-Os^{II}$ couples of $(tpm)(Cl)_2Os^{II}(N_2)Os^{II}(Cl)_2(tpm)$.[8] Following an oxidative scan past the $Os^{III}-Os^{III}/Os^{III}-Os^{II}$ wave, reversible waves at $E_{1/2} = +1.40$ and -0.08 V vs SSCE ($\Delta E_{1/2} = 1.48$ V) appear for the $Os^{IV/III}$ and $Os^{III/II}$ couples of $[Os^{III}(tpm)(Cl)_2(NCCH_3)]^+$.[6] These observations are consistent with eq 8

$$[Os^{VI}(tpm)(Cl)_2(N)]^+ + e^- \rightarrow \{Os^{V}(tpm)(Cl)_2(N)\} \rightarrow 1/2(tpm)(Cl)_2Os^{II}(N_2)Os^{II}(Cl)_2(tpm) \quad (8)$$

and loss of μ-N_2 upon oxidation to the $Os^{III}-Os^{III}$ dimer

$$(tpm)(Cl)_2Os^{II}(N_2)Os^{II}(Cl)_2(tpm) \xrightarrow{-2e^-} [(tpm)(Cl)_2Os^{III}(N_2)Os^{III}(Cl)_2(tpm)]^{2+} \quad (9a)$$

$$[(tpm)(Cl)_2Os^{III}(N_2)Os^{III}(Cl)_2(tpm)]^{2+} + 2CH_3CN \rightarrow 2[Os^{III}(tpm)(Cl)_2(NCCH_3)]^+ + N_2 \quad (9b)$$

Similar observations were made for **2**. An irreversible $Os^{VI/V}$ reduction is observed at $E_{p,c} = -0.98$ V vs SSCE, followed by reversible oxidative waves at $E_{1/2} = -0.20$ and $+0.35$ V vs SSCE for the $Os^{III}-Os^{II}/Os^{II}-Os^{II}$ and $Os^{III}-Os^{III}/Os^{III}-Os^{II}$ couples of $[(Tp)(Cl)_2Os^{II}(N_2)Os^{II}(Cl)_2(Tp)]^{2-}$ consistent with eq 10. In addition, reversible couples at $E_{1/2} = +0.76$ and -0.45 V vs SSCE ($\Delta E_{1/2} = 1.21$ V) are observed for the $Os^{IV/III}$ and $Os^{III/II}$ couples of $[Os^{II}(Tp)(Cl)_2(NCCH_3)]^-$. These waves appear before oxidation to $Os^{III}(N_2)Os^{III}$. This points to partial decomposition of $[(Tp)(Cl)_2Os^{II}(N_2)Os^{II}(Cl)_2(Tp)]^{2-}$ to give $[Os^{II}(Tp)(Cl)_2(NCCH_3)]^-$ and N_2.

$$Os^{VI}(Tp)(Cl)_2(N) + e^- \rightarrow \{[Os^{V}(Tp)(Cl)_2(N)]^-\} \rightarrow 1/2[(Tp)(Cl)_2Os^{II}(N_2)Os^{II}(Cl)_2(Tp)]^{2-} \quad (10)$$

In cyclic voltammograms of $[Os^{III}(tpm)(Cl)_2(NH_3)]^+$ (**3**) in CH_3CN 0.1 M in TBAH (Figure 5, upper part) chemically reversible waves appear at $E_{1/2} = -0.35$ and $+1.22$ V vs SSCE for the $Os^{III/II}$ and $Os^{IV/III}$ couples (Figure 5a). After addition of 10-fold excess of bpy (Figure 5b,c), the $Os^{IV/III}$ wave (wave I) becomes chemically irreversible at $E_{p,a} = +1.14$ V. It is followed by an irreversible oxidation wave at $E_{p,a} = +1.50$ V (wave II). On a reverse scan, reductive waves appear at $E_{p,c} = +0.11$ V (wave A) and a broad wave at $E_{p,c} \sim -0.53$ V (wave B). When the reductive scan is reversed past the first oxidative wave, only wave A appears.

A similar behavior is observed for **4** (Figure 5, lower part). Reversible waves for the $Os^{III/II}$ and $Os^{IV/III}$ couples appear at $E_{1/2} = -0.86$ and $+0.83$ V vs SSCE (Figure 5a). Upon addition of a 10-fold excess of bpy, the $Os^{IV/III}$ wave remains quasi-irreversible at $E_{1/2} = +0.70$ V (Figure 5b). It is followed by a second oxidation wave at $E_{p,a} = +1.22$ V (wave II). On a reverse scan past this wave, irreversible Os^{VI}−nitrido reduction is observed at $E_{p,c} = -0.55$ V (wave B). If the scan is reversed past wave I (Figure 5c), wave A appears at $E_{p,c} = +0.62$ V, and there is no sign of wave B.

Electrochemistry in Water. Cyclic voltammograms of **1a**, **2**, **3**, and **4** in 3 M HCl are available as Supporting Information. For **1a**, a multielectron reduction wave appears at $E_{p,c} = -0.33$ V vs SSCE. Upon scan reversal, the $Os^{III/II}$ couple appears at $E_{p,a} = -0.31$ V, and the $Os^{IV/III}$ couple appears at $E_{1/2} = +0.95$ V. The peak current ratio $i_{p,c}/i_{p,a}$ is less than 1 for the $Os^{IV/III}$ couple, suggesting a reaction competitive with reduction of Os^{IV}.

(19) Demadis, K. D.; El-Samanody E.-S.; Meyer, T. J.; White, P. S. *Polyhedron* **1999**, *18*, 1587 and references therein.
(20) House, D. A. In *Comprehensive Coordination Chemistry*; Wilkinson, G., Gillard, R. D., McCleverty, J. A., Eds.; Pergamon Press: Oxford, 1987; Vol. 2, Section 13.1.2.
(21) (a) Griffith, W. P. *Coord. Chem. Rev.* **1972**, *8*, 269. (b) Dehnicke, K.; Strahle, J. *Angew Chem., Int. Ed. Engl.* **1992**, *31*, 955.
(22) Schmidt, K. H.; Muller, A. *Coord. Chem. Rev.* **1976**, *19*, 41.
(23) (a) Schmidt, K. H.; Hauswirth, W.; Muller, A. *J. Chem. Soc., Dalton Trans.* **1975**, 2199. (b) Siebert, H.; Eysel, H. H. *J. Mol. Struct.* **1969**, *4*, 29.
(24) Schimidt, K. H.; Muller, A. *J. Mol. Struct.* **1974**, 29.
(25) Williams, D. S.; Coia, G. M.; Meyer, T. J. *Inorg. Chem.* **1995**, *34*, 586.
(26) (a) Llobet, A.; Hodgson, D. J.; Meyer, T. J. *Inorg. Chem.* **1990**, *29*, 3760. (b) Llobet, A.; Doppelt, P.; Meyer, T. J. *Inorg. Chem.* **1988**, *27*, 514.

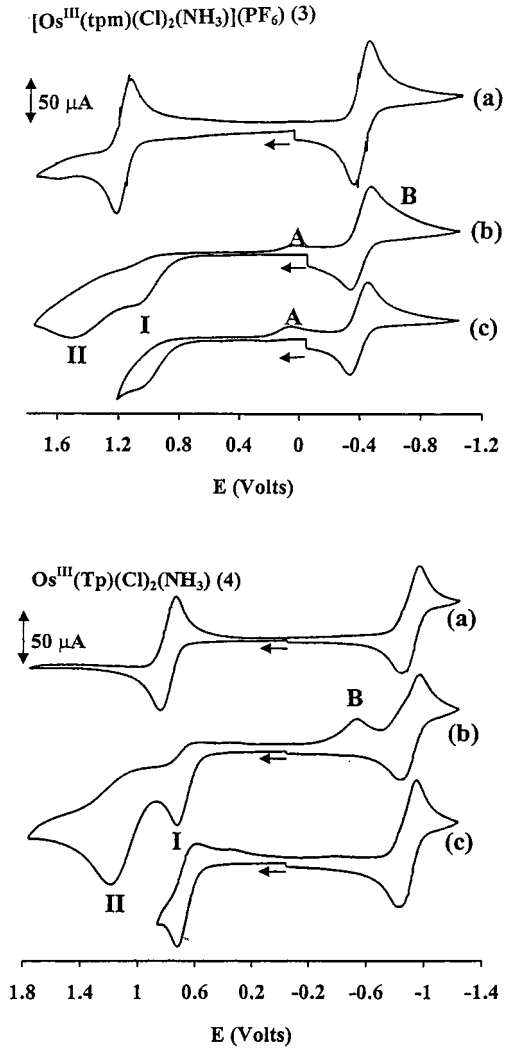

Figure 5. Cyclic voltammograms of **3** and **4** in CH_3CN (0.1 M TBAH) at a Pt disk working electrode at a scan rate of 200 mV/s vs SSCE. Panels b and c are voltammograms after addition of a 10-fold excess of bpy.

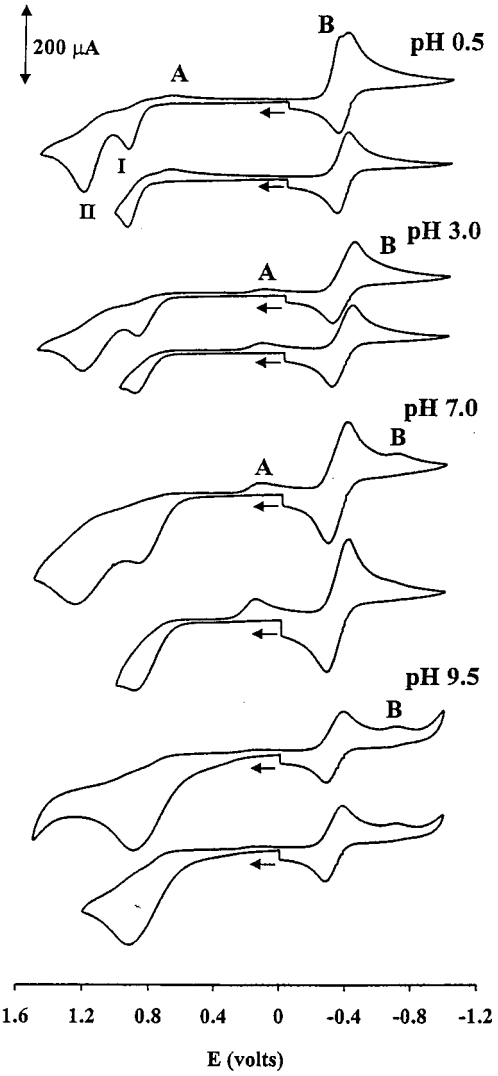

Figure 6. Cyclic voltammograms of **3** in 1:1 (v:v) $CH_3CN:H_2O$, 0.1 M in TBAH at different pH values at a glassy carbon working electrode at a scan rate of 200 mV/s vs SSCE.

For **2**, irreversible nitrido reduction occurs at $E_{p,c} = -0.70$ V vs SSCE, followed by the $Os^{III/II}$ couple of Os^{II}−ammine at $E_{1/2} = -0.79$ V and on reverse scan, a reversible $Os^{IV/III}$ wave at $E_{1/2} = +0.71$ V. For **3**, waves for the $Os^{III/II}$ couple appear at $E_{1/2} = -0.35$ V; for the $Os^{IV/III}$ couple they appear at $E_{1/2} = +0.95$ V with $(i_{p,c}/i_{p,a})$ <1 for the latter. There is no evidence for further Os(IV→VI) oxidation to the onset of background oxidation of Cl^-. On a reverse scan, the irreversible nitrido reduction wave appears as a shoulder at $E_{p,c} = -0.32$ V. For **4**, reversible waves are observed at $E_{1/2} = -0.79$ and +0.72 V for the $Os^{III/II}$ and $Os^{IV/III}$ couples, respectively. Because of solubility limitations, the pH dependence of the couples were investigated in 1:1 (v:v) $CH_3CN:H_2O$, 0.1 M in TBAH. Potential measurements in this mixed-solvent medium gave the same values within experimental error as in aqueous solutions at the same pH.[27]

Cyclic voltammograms of solutions containing **3** are shown in Figure 6. At pH 0.5, the Os(III→IV) oxidation (wave I) at $E_{p,a} = +0.84$ V is followed by Os(IV→VI) oxidation (wave II) at $E_{p,a} = +1.25$ V. On scan reversal, a reduction wave is observed at $E_{p,c} = +0.69$ V (wave A) and a nitrido reduction at $E_{p,c} = -0.31$ V (wave B). When the oxidative scan is halted after wave I, wave B does not appear. wave A is independent of scan rate from 50 to 500 mV/s.

As the pH is increased, the same pattern of waves is observed, although by pH 9.5, the Os(IV→VI) wave has shifted and overlaps the Os(III→IV) wave.

For **4** at pH 0.5 (Figure 7), the $Os^{IV/III}$ couple is chemically reversible, $E_{1/2} = +0.72$ V (wave I), and Os(IV→VI) oxidation occurs at $E_{p,a} = +1.14$ V (wave II). Scanning through this wave results in two-electron oxidation of Os^{IV} to the Os^{VI}−nitrido complex. On scan reversal, Os(VI→III) reduction is observed at $E_{p,c} = -0.62$ V (wave B) and the reversible wave for the $Os^{III/II}$ couple. At pH 7.5, Os(III→IV) oxidation is chemically irreversible, and wave A appears at $E_{p,c} = -0.25$ V. wave B only appears after scanning through the Os(IV→VI) wave.

Discussion

In aqueous solution, both **3** and **4** undergo reversible $4e^-/3H^+$ oxidation to $Os^{VI}{\equiv}N$ forms. This is a reactivity shared with *cis*- and *trans*-$[Os^{III}(tpy)(Cl)_2(NH_3)]^+$ and a product of the relatively electron-rich coordination environments in these

(27) Huynh, M. H. V.; Meyer, T. J. Unpublished results.

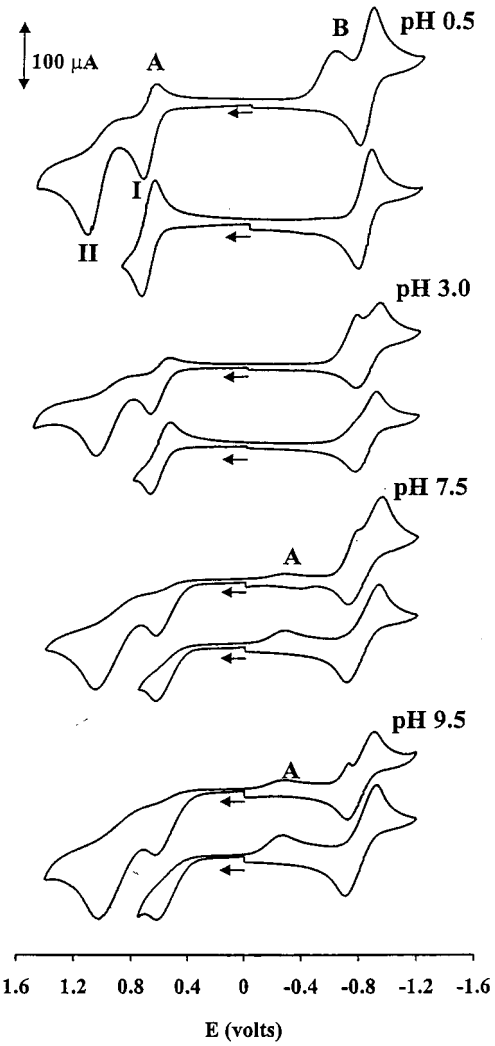

Figure 7. As in Figure 6 but for **4**.

complexes.[3a] In less electron-rich environments, further hydration and oxidation gives nitrosyls.

$$[Os^{III}(tpm)(Cl)_2(NH_3)]^+ \underset{+3e^-,\,+3H^+}{\overset{-3e^-,\,-3H^+}{\rightleftharpoons}} [Os^{VI}(tpm)(Cl)_2(N)]^+ \quad (11)$$

The reactions occur stepwise with Os(II→III) oxidation followed by further oxidation to Os^{IV}.

$$Os^{III}(Tp)(Cl)_2(NH_3) \underset{+3e^-,\,+3H^+}{\overset{-3e^-,\,-3H^+}{\rightleftharpoons}} Os^{VI}(Tp)(Cl)_2(N) \quad (12)$$

The Os^{II} forms of both complexes are accessible by cyclic voltammetry but are air sensitive, and the Os^{III} forms are separated after reduction of the corresponding nitrido complexes and work up of the product.

The structures of **3** and **4** are as expected for complexes of this type. The Os−Cl bond distances fall in a normal range for Os^{III} complexes.[19] The structure of the nitrido precursor, $[Os^{VI}(tpm)(Cl)_2(N)]^+$, is complicated by random disorder in the crystal caused by occupation of adjacent coordination sites by the chloride and nitrido ligands. Consequently, the bond length Os−Cl/N(3) of 1.887(10) Å in Table 2 represents an upper limit on the actual Os−N bond distance. For comparison, Os−N(nitrido) bond distances are 1.663(5) and 1.652(4) Å in *trans*-$[Os^{VI}(tpy)(Cl)_2(N)]^+$ [2a] and *cis*-$[Os^{VI}(tpy)(Cl)_2(N)]^+$,[28] respectively. The coordination of the tpm and Tp^- ligands is normal with no unexpected features.[19,29]

Table 3. Redox Potentials for $Os^{III/II}$ and $Os^{IV/III}$ Couples in CH_3CN (0.1 M in TBAH) vs SSCE

	$E_{1/2}$		
complex	$Os^{III/II}$	$Os^{IV/III}$	ref
$[Os^{II}(tpy)(bpy)(NH_3)]^{2+}$	+0.68	−	1, 3
cis-$[Os^{II}(bpy)_2(Cl)(NH_3)]^+$	+0.21	+1.69[a]	3
trans-$[Os^{III}(tpy)(Cl)_2(NH_3)]^+$	−0.10	+1.18	2
cis-$[Os^{III}(tpy)(Cl)_2(NH_3)]^+$	−0.11	+1.18	3
$[Os^{III}(tpm)(Cl)_2(NH3)]^+$ (**3**)	−0.35	+1.22	this work
$Os^{III}(Tp)(Cl)_2(NH_3)$ (**4**)	−0.86	+0.83	this work

[a] Irreversible oxidation, $E_{p,a}$, is cited.

The d^2 nitrido complexes **1** and **2** are diamagnetic as expected with $\nu(Os{\equiv}^{14}N)$ appearing at 1068 cm^{-1} for **2**[13] (1038 cm^{-1} for $Os{\equiv}^{15}N$ in **2***) and at 1074 cm^{-1} for **1a** (1053 cm^{-1} for $\nu(Os{\equiv}^{15}N)$ in **1***). Interconfigurational $d\pi \rightarrow d\pi$ bands are observed for both nitrido complexes in the visible spectrum at ~450 nm.

As shown by the data in Table 3, the addition of these examples extends the range of potentials for the $Os^{IV/III}$ and $Os^{III/II}$ couples of polypyridyl−ammine complexes of Os over an impressive range with an important role played by simple replacement of polypyridyl ligands by Cl^- and of tpm by its anionic analogue Tp^-.

The appearance of reversible electron transfer depends on the medium. The $Os^{IV/III}$ and $Os^{III/II}$ couples are chemically reversible in dry CH_3CN or strong acid. Irreversible oxidation of coordinated NH_3 requires proton loss and occurs in water or after addition of a base to CH_3CN.

Electrochemistry in CH_3CN. Electrochemical reduction of **1a** in CH_3CN occurs by one electron at $E_{p,c} = -0.47$ V (Figure 5), is chemically irreversible, and gives $(tpm)(Cl)_2Os^{II}(N_2)Os^{II}(Cl)_2(tpm)$ (eq 8). The product, which was synthesized earlier by cobaltocene reduction of **2** in dry CH_2Cl_2, eq 13,[7] was characterized by its electrochemical and spectral properties.

$$[Os^{VI}(tpm)(Cl)_2(N)]^+ + Cp_2Co \rightarrow 1/2(tpm)(Cl)_2Os^{II}(N_2)Os^{II}(Cl)_2(tpm) + [Cp_2Co]^+ \quad (13)$$

Reduction of **2** gives $[(Tp)(Cl)_2Os^{II}(N_2)Os^{II}(Cl)_2(Tp)]^{2-}$, whose mixed-valence form has been prepared by cobaltocene reduction[7]

$$2Os^{VI}(Tp)(Cl)_2(N) + Cp_2Co \rightarrow [(Tp)(Cl)_2Os^{III}(N_2)Os^{II}(Cl)_2(Tp)](Cp_2Co) \quad (14)$$

Also shown in Figure 5 is the dramatic change that accompanies addition of a 10-fold excess of bpy added as a base. The Os(III→IV) oxidation wave for **3** shifts from +1.22 to +1.14 V and becomes irreversible. A new wave appears on

(28) Huynh, M. H. V.; Demadis, K. D.; Meyer, T. J.; White, P. S. Manuscript in preparation.
(29) (a) Koch, J. L.; Shapley, P. A. *Organometallics* **1997**, *16*, 4071. (b) Schrock, R. R.; Lapointe, A. M. *Organometallics* **1993**, *12*, 3379. (c) Lapointe, A. M.; Schrock, R. R.; Davies, W. M. *J. Am. Chem. Soc.* **1995**, *117*, 4802. (d) Bohanna, C.; Esteruelas, M. A.; Martinez, M.-P. *Organometallics* **1997**, *16*, 4464. (e) Trofimenko, S. *Chem. Rev.* **1993**, *93*, 943. (f) Trofimenko, S. *Prog. Inorg. Chem.* **1986**, *34*, 115. (g) Laurent, F.; Plantalech, E.; Donnadieu, B.; Jiménez, A.; Hernández, F.; Martínez-Ripoll, M.; Biner, M.; Llobet, A. *Polyhedron* **1999**, *18*, 3321. (h) Trofimenko, S. *The Coordination Chemistry of Polypyrazolylborate Ligands*; Imperial College Press: River Edge, NJ, 1999.

the reverse scan at $E_{p,c} = +0.10$ V (wave A). The shift in potential with added bpy is consistent with deprotonation of Os^{III} followed by oxidation to Os^{IV} [3a]

$$[Os^{III}(tpm)(Cl)_2(NH_3)]^+ + p\text{bpy} \rightleftharpoons [Os^{III}(tpm)(Cl)_2(NH_{3-p})]^{1-p} + p\text{bpyH}^+ \quad (15)$$

$$[Os^{III}(tpm)(Cl)_2(NH_{3-p})]^{1-p} \xrightarrow[(p = 1 \text{ or } 2)]{-e^-} [Os^{IV}(tpm)(Cl)_2(NH_{3-p})]^{2-p} \quad (16)$$

The proton composition of Os^{IV} is unknown, but oxidation of *cis*- and *trans*-$[Os^{III}(tpy)(Cl)_2(NH_3)]^+$ appears to give $[Os^{IV}(tpy)(Cl)_2(NH_2)]^+$.[3a]

With added bpy, the Os^{IV} intermediate undergoes further irreversible oxidation at $E_{p,a} = +1.50$ V (wave II) (Figure 5). The product is $[Os^{VI}(tpm)(Cl)_2(N)]^+$, as shown by the appearance of the characteristic, irreversible Os(VI→V) reduction at $E_{p,c} \sim -0.53$ V (wave B). There is no evidence for Os^V as an intermediate in the cyclic voltammgrams, and the net reaction appears to be

$$[Os^{IV}(tpm)(Cl)_2(NH_{3-p})]^{2-p} + m\text{bpy} \xrightarrow[(m = 1 \text{ or } 2)]{-2e^-} [Os^{VI}(tpm)(Cl)_2(N)]^+ + m\text{bpyH}^+ \quad (17)$$

In cyclic voltammograms of **4** with added bpy (Figure 5b,c), the $Os^{IV/III}$ wave at $E_{p,a} = +0.70$ V continues to appear at $E_{1/2} = 0.83$ V. However, irreversible Os(IV→VI) oxidation occurs at $E_{p,a} = +1.20$ V (wave II in Figure 5). Os(IV→III) re-reduction is in competition with reduction of a new intermediate at $E_{p,c} \sim +0.3$ V (wave A). Under these conditions, oxidation to $[Os^{IV}(Tp)(Cl)_2(NH_3)]^+$ is followed by proton loss to give $[Os^{IV}(Tp)(Cl)_2(NH_{3-p})]^{(1-p)+}$, which occurs on the cyclic voltammetry time scale.[3a]

$$[Os^{IV}(Tp)(Cl)_2(NH_3)] + 3\text{bpy} \xrightarrow{-2e^-} Os^{VI}(Tp)(Cl)_2(N) + 3\text{bpyH}^+ \quad (18)$$

Subsequent Os(VI→III) re-reduction at $E_{p,c} = -0.55$ V (wave B) occurs on reverse scan. This is a significant observation since, in CH_3CN, reduction of either **1** or **2** gives the corresponding $Os^{II}(N_2)Os^{II}$ complexes (eqs 8 and 10). These reactions occur by initial one-electron reduction

$$[Os^{IV}(L)_3(Cl)_2(N)]^{+ \text{ or } 0} \xrightarrow{-2e^-} [Os^{V}(L)_3(Cl)_2(N)]^{0 \text{ or } -} \quad (19)$$

followed by N···N coupling.[7,9,10]

The difference in behavior with added bpy (and $bpyH^+$ after an oxidative scan) suggests that Os(VI→V) reduction in the presence of $bpyH^+$ results in protonation before N···N coupling can occur

$$[Os^{VI}(Tp)(Cl)_2(N)]^0 + e^- \rightarrow \{Os^{V}(Tp)(Cl)_2(N)\}^- \xrightarrow{+\text{bpyH}^+} [Os^{V}(Tp)(Cl)_2(NH)]^0 + \text{bpy} \quad (20)$$

$$[Os^{VI}(Tp)(Cl)_2(N)]^0 + 2e^- + 2\text{bpyH}^+ \rightarrow [Os^{V}(Tp)(Cl)_2(NH_3)]^0 + \text{bpy} \quad (21)$$

In support of this conclusion, in an independent experiment, electrochemical reduction of **1a** in CH_3CN with added HPF_6 also gave the ammine complex as shown by cyclic voltammetry.

Electrochemistry of $[Os^{VI}(tpm)(Cl)_2(N)]^+$ and $[Os^{III}(tpm)(Cl)_2(NH_3)]^+$ in Water. In 3 M HCl, **1a** undergoes multielectron reduction at $E_{p,c} = -0.33$ V. The product is $Os^{II}(tpm)(Cl)_2(NH_3)$, as shown by cyclic voltammetry, with $E_{1/2}$ ($Os^{III/II}$) = −0.31 and $E_{1/2}$ ($Os^{IV/III}$) = +0.95 V.

Oxidation of $[Os^{III}(tpm)(Cl)_2(NH_3)]^+$ to Os^{IV} occurs at $E_{1/2} = +0.95$ V, but at a scan rate of 20 mV/s, re-reduction to Os^{III} is incomplete (Supporting Information, Figure 1). The peak current ratio $i_{p,c}/i_{p,a}$ is <1 for the $Os^{IV/III}$ couple, and the Os^{VI}–nitrido reduction wave appears at $E_{p,c} = -0.32$ V. These observations point to the instability of $[Os^{IV}(tpm)(Cl)_2(NH_3)]^{2+}$ toward disproportionation on the seconds time scale of the cyclic voltammetry experiments (eq 22).

$$3[Os^{IV}(tpm)(Cl)_2(NH_3)]^{2+} \rightarrow 2[Os^{III}(tpm)(Cl)_2(NH_3)]^+ + [Os^{IV}(tpm)(Cl)_2(N)]^+ + 3H^+ \quad (22)$$

As the pH is increased, the Os(III→IV) oxidation becomes chemically irreversible. The oxidative component of the voltammetric wave is pH-dependent with $E_{p,a}$ decreasing by ∼45 mV/pH unit from pH 0.5 to pH 3.0. The Os(IV→III) re-reduction is also pH-dependent from pH 0.5 to pH 3.0 with $E_{p,c} = +0.69$ V (wave A) at pH 0.5 and $E_{p,c} = +0.11$ V at pH 3.0. From pH 3.0 to pH 7.0, wave A is pH-independent.

The observations from pH 0.5 to pH 3.0 are qualitatively consistent with a change in mechanism from oxidation to Os^{IV} followed by proton loss (eqs 23 and 24)

$$[Os^{III}(tpm)(Cl)_2(NH_3)]^+ \underset{+e^-}{\overset{-e^-}{\rightleftharpoons}} [Os^{IV}(tpm)(Cl)_2(NH_3)]^{2+} \quad (23)$$

$$[Os^{IV}(tpm)(Cl)_2(NH_3)]^{2+} \underset{(q = 1 \text{ or } 2)}{\rightleftharpoons} [Os^{IV}(tpm)(Cl)_2(NH_{3-q})]^{(2-q)} + q\text{H}^+ \quad (24)$$

to rate-limiting deprotonation of Os^{III} with OH^- as the base (rather than H_2O).[3a]

$$[Os^{III}(tpm)(Cl)_2(NH_3)]^+ + q\text{OH}^- \underset{(q = 1 \text{ or } 2)}{\rightleftharpoons} [Os^{III}(tpm)(Cl)_2(NH_{3-q})]^{(1-q)+} + q\text{H}_2\text{O}^+ \quad (25)$$

$$[Os^{III}(tpm)(Cl)_2(NH_{3-q})]^{(1-q)+} \underset{+e^-}{\overset{-e^-}{\rightleftharpoons}} [Os^{IV}(tpm)(Cl)_2(NH_{3-q})]^{(2-q)+} \quad (26)$$

The Os(IV→VI) wave at $E_{p,a} = +1.25$ V (wave II in Figure 6) is pH-independent from pH 0.5 to pH 7.0, but the Os(VI→IV) reduction is pH-dependent. $E_{p,c}$ varies ∼45 mV/pH unit.

This pH dependence is consistent with rate-limiting Os(IV→VI) oxidation followed by proton loss (eqs 27 and 28).[3a]

$$[Os^{IV}(tpm)(Cl)_2(NH_2)]^+ \underset{+2e^-}{\overset{-2e^-}{\rightleftharpoons}} [Os^{VI}(tpm)(Cl)_2(NH_2)]^{3+} \quad (27)$$

$$[Os^{VI}(tpm)(Cl)_2(NH_2)]^{3+} \rightleftharpoons [Os^{VI}(tpm)(Cl)_2(N)]^+ + 2H^+ \quad (28)$$

The variation in $E_{p,c}$ of ∼45 mV/pH unit is consistent with a $2e^-/2H^+$ couple based on the Nernst equation, eq 29, in which $E_{1/2}$ is the half-wave potential and m and n are the number of protons and electrons transferred, respectively.[3a]

$$E = E_{1/2} - 0.059m/n \text{ pH} \quad (29)$$

This suggests that the proton composition at Os^{IV} is $[Os^{IV}(tpm)(Cl)_2(NH_2)]^+$ ($q = 1$ in eqs 12, 25, and 26). The same conclusion was reached for Os^{IV} in *cis*- and *trans*-$[Os^{IV}(tpy)(Cl)_2(NH_2)]^+$ based on pH-dependent electrochemical measurements.[3a]

Above pH 7.0, the Os(IV→VI) wave becomes pH-dependent, and the Os(VI→IV) wave at $E_{p,c} = -0.75$ is pH-independent. By pH 9.5, the Os(IV→VI) wave overlaps the Os(III → IV) wave and only a single, three-electron wave is observed at $E_{p,a} = 0.97$ V.

The change in behavior for the two couples above pH 7.0 points to a change in mechanism. Above pH 7.0, the pH dependence is consistent with initial deprotonation at Os^{IV} by OH^- acting as the base (eq 30) followed by two-electron oxidation (eq 31).

$$[Os^{IV}(tpm)(Cl)_2(NH_2)]^+ + 2OH^- \rightleftharpoons [Os^{IV}(tpm)(Cl)_2(N)]^- + 2H_2O \quad (30)$$

$$[Os^{IV}(tpm)(Cl)_2(N)]^- \underset{+2e^-}{\overset{-2e^-}{\rightleftharpoons}} [Os^{VI}(tpm)(Cl)_2(N)]^+ \quad (31)$$

There is no evidence at any pH for Os^{V} as an intermediate.

Electrochemistry of $Os^{VI}(Tp)(Cl)_2(N)$ and $Os^{III}(Tp)(Cl)_2(NH_3)$ in 1:1 (v:v) CH_3CN:H_2O. In 1:1 (v:v) CH_3CN:3 M HCl, reduction of $Os^{VI}(Tp)(Cl)_2(N)$ (**2**) occurs at $E_{p,c} = -0.70$ V to give **3**. The $Os^{IV/III}$ and $Os^{III/II}$ couples for **4** are chemically reversible and appear at $E_{1/2} = +0.72$ and -0.79 V, respectively.

From the results in Figure 7, oxidation of **4** to $[Os^{IV}(Tp)(Cl)_2(NH_3)]^+$ is chemically reversible until pH 6.0. Above pH 6.0, Os(III→IV) oxidation leads to a new wave for Os(IV→III) reduction (wave A in Figure 7) at $E_{p,c} = -0.25$ V. Both waves are independent or only slightly dependent on pH up to pH 9.5. This pH dependence is consistent with rate-limiting oxidation to Os^{IV} followed by proton loss with OH^- acting as the base (eqs 32 and 33).

$$Os^{III}(Tp)(Cl)_2(NH_3) \underset{+e^-}{\overset{-e^-}{\rightleftharpoons}} [Os^{IV}(Tp)(Cl)_2(NH_3)]^+ \quad (32)$$

$$[Os^{IV}(Tp)(Cl)_2(NH_3)]^+ + rOH^- \underset{(r = 1 \text{ or } 2)}{\rightleftharpoons} [Os^{IV}(Tp)(Cl)_2(NH_{3-r})]^{(1-r)} + rH_2O \quad (33)$$

Oxidation of Os^{IV} to Os^{VI} occurs at $E_{p,a} \sim +1.14$ V and is independent of pH from pH 0.5 to pH 9.5. Os(VI→IV) reduction is pH-dependent between pH 0.5 and pH 3.0 with $E_{p,c}$ decreasing ~45 mV/pH unit consistent with $2e^-/2H^+$ reduction. These observations point to $r = 1$ in eq 33 and rate-determining Os(IV→VI) oxidation followed by loss of two protons in eqs 34 and 35.

$$Os^{IV}(Tp)(Cl)_2(NH_2) \underset{+2e^-}{\overset{-2e^-}{\rightleftharpoons}} [Os^{VI}(Tp)(Cl)_2(NH_2)]^{2+} \quad (34)$$

$$[Os^{VI}(Tp)(Cl)_2(NH_2)]^{2+} \rightleftharpoons Os^{VI}(Tp)(Cl)_2(N) + 2H^+ \quad (35)$$

Neither Os(IV→VI) oxidation nor Os(VI→IV) reduction is pH-dependent from pH 3.0 to pH 9.5. This is consistent with rate-limiting oxidation followed by proton loss with OH^- acting as the base (eqs 36 and 37).

$$Os^{IV}(Tp)(Cl)_2(NH_2) \underset{+2e^-}{\overset{-2e^-}{\rightleftharpoons}} [Os^{VI}(Tp)(Cl)_2(NH_2)]^{2+} \quad (36)$$

$$[Os^{VI}(Tp)(Cl)_2(NH_2)]^{2+} + 2OH^- \rightleftharpoons Os^{VI}(Tp)(Cl)_2(N) + 2H_2O \quad (37)$$

Conclusions

Our results demonstrate that the interconversion between Os^{III}−ammine and Os^{VI}−nitrido forms is reversible for the tpm and Tp^- complexes. In contrast to oxidation of *cis*-$[Os^{III}(bpy)_2(Cl)(NH_3)]^{2+}$,[3] there is no evidence for nitrosyl formation or N···N coupling to give μ-N_2 bridging products. In their chemical reversibility, they are analogous to the *cis*- and *trans*-$[Os^{VI}(tpy)(Cl)_2(N)]^+/[Os^{III}(tpy)(Cl)_2(NH_3)]^{+}$[2,3] and related aqua/oxo couples, such as *trans*-$[Ru^{VI}(tpy)(O)_2(H_2O)]^{2+}/[Ru^{III}(tpy)(H_2O)_2(OH)]^{2+}$.[30]

The key to stabilization of the high oxidation state in these cases is proton loss and multiple bonding. For the Ru(VI) example, the high oxidation state is accessible through the stabilization provided by the formation of two Ru═O interactions in the trans dioxo structure. For Os(VI), proton loss and triple bond formation are sufficient to stabilize Os(VI).

For the tpm and Tp^- examples, the coordination environments are sufficiently electron rich that both $Os^{III/II}$ and $Os^{IV/III}$ couples are accessible in CH_3CN or strong acid, within the solvent limits, without proton loss. The impact of ligands on the potentials of the $Os^{III/II}$ and $Os^{IV/III}$ couples can be clearly seen in the data in Table 3 and the decreases of 0.51 and 0.39 V for $Os^{III}(Tp)(Cl)_2(NH_3)$ as compared to $[Os^{III}(tpm)(Cl)_2(NH_3)]^+$. Electron content at the metal also plays an important role in the chemistry. The Os^{IV}−nitrido/Os^{III}−ammine reversibility is lost in more electron deficient coordination environments such as $[Os^{III}(tpy)(bpy)(NH_3)]^{3+}$ and *cis*-$[Os^{III}(bpy)_2(Cl)(NH_3)]^{2+}$. In these cases, oxidation to Os^{IV} is followed by hydration at the N atom and further oxidation to nitrosyl or to N···N coupling for the latter.[3]

Oxidation of $[Os^{III}(tpm)(Cl)_2(NH_3)]^+$ to Os^{IV} is followed by rapid proton loss to give $Os^{IV}NH_2^+$, even at pH 0.5. For $Os^{III}(Tp)(Cl)_2(NH_3)$, the $Os^{IV/III}$ couple remains chemically reversible up to pH 6.0. This is a consequence of decreased Os^{IV}−NH_3 acidity in the more electron-rich coordination environment provided by the Tp^- ligand.

In the oxidation of coordinated ammonia to nitrido, the kinetic bottleneck is at the Os(III → IV) stage. At this stage, there is a requirement for proton loss before further oxidation can occur. The details depend on the complex and the pH. For $Os^{III}(Tp)(Cl)_2(NH_3)$ from pH 0.5 to pH 9.5, oxidation of Os^{III} to Os^{IV} precedes proton loss. It is followed by proton loss to OH^- as a base above pH 6.0. For $[Os^{III}(tpm)(Cl)_2(NH_3)]^+$ from pH 0.5 to pH 3.0, there is a transition from rate-limiting oxidation, followed by proton loss, to rate-limiting loss of protons from Os^{III} to OH^- as a base.

Acknowledgment. Acknowledgments are to the National Science Foundation for Grant CHE-9503738 and to Dr. My Hang V. Huynh of the Los Alamos National Laboratories for help with editing the manuscript. E.-S. E.-S. thanks the Egyptian Government for the data collection grant.

Note Added in Proof: While this paper was in press Mayer et al. (C−N Bond Formation on Addition of Aryl Carbanions to the Electrophilic Nitrido Ligand in $TpOs(N)Cl_2$, *J. Am. Chem. Soc.* **2001**, *123*, 1059) reported the crystal structure of $TpOs(N)Cl_2$. They have observed a N/Cl disorder (73% N, 23% Cl) in the structure of $TpOs(N)Cl_2$ similar to that in $[Os^{VI}(tpm)$-

(30) Dovletoglou, A.; Adeyemi, S. A.; Lynn, M. H.; Hodgson, D. J.; Meyer, T. J. *J. Am. Chem. Soc.* **1990**, *112*, 8989. (b) Adeyemi, S. A.; Dovletoglou, A.; Gaudalupe, A.; Meyer, T. J. *Inorg. Chem.* **1992**, *32*, 1375.

$(N)(Cl)_2](BF_4)$ (**1b**), in the present paper. As indicated, cocrystallization of $Os(Cl)_3$(Tp or tpm) impurities is the probable cause of this disorder.

Supporting Information Available: Cyclic voltammograms of **1a**, **2**, **3**, and **4** in 3 M HCl, additional details of the crystallographic analysis of the compounds **1b**, **3**, and **4**, fully labeled ORTEP diagrams, tables of atomic coordinates, isotropic thermal parameters, and bond distances and angles. This material is available free of charge via the Internet at http://pubs.acs.org.

IC000764F